Phenylene ring dynamics in bisphenol-A-polysulfone by neutron scattering

S. Arrese-Igor
Departamento de Física de Materiales UPV/EHU, Apartado 1072, 20080 San Sebastián, Spain

A. Arbe
Unidad Física de Materiales (CSIC-UPV/EHU), Apartado 1072, 20080 San Sebastián, Spain

A. Alegría
Departamento de Física de Materiales UPV/EHU, Apartado 1072, 20080 San Sebastián, Spain and Unidad Física de Materiales (CSIC-UPV/EHU), Apartado 1072, 20080 San Sebastián, Spain

J. Colmenero[a)]
Departamento de Física de Materiales UPV/EHU, Apartado 1072, 20080 San Sebastián, Spain, Donostia International Physics Center, Paseo Manuel Lardizabal 4, 20018 San Sebastián, Spain, and Unidad Física de Materiales (CSIC-UPV/EHU), Apartado 1072, 20080 San Sebastián, Spain

B. Frick
Institut Laue-Langevin, BP 156X, 38042 Grenoble Cedex 9, France

(Received 6 August 2003; accepted 6 October 2003)

We have investigated the dynamics of phenylene rings in a glassy polysulfone (bisphenol-A-polysulfone) by means of quasielastic neutron scattering. Nowadays it is well known that these molecular motions are directly connected with the mechanical properties of engineering thermoplastics in general. The particular system investigated by us has the advantage that by selective deuteration of the methyl groups, the neutron scattering measured is dominated by the incoherent contribution from the protons in the phenylene rings. In this way, the dynamics of such molecular groups can be experimentally isolated. Two different types of neutron spectrometers: time of flight and backscattering, were used in order to cover a wide dynamic range, which extends from microscopic (10^{-13} s) to mesoscopic (10^{-9} s) times. Moreover, neutron diffraction experiments with polarization analysis were also carried out in order to characterize the structural features of the sample investigated. Fast oscillations of increasing amplitude with temperature and π-flips are identified for phenylene rings motions. Due to the structural disorder characteristic of the amorphous state, both molecular motions display a broad distribution of relaxation times, which spreads over several orders of magnitude. Based on the results obtained, we propose a model for phenylene rings dynamics, which combines the two kinds of molecular motions identified. This model nicely describes the neutron scattering results in the whole dynamic range investigated. [DOI: 10.1063/1.1630013]

I. INTRODUCTION

Engineering thermoplastics have an important technological significance owing to their good mechanical and thermal properties that make them suitable for a huge number of applications. Their interesting ultimate mechanical properties are probably related to the ability of these polymers to accommodate a stress with highly activated molecular motions. This is why considerable efforts have been made to identify the molecular origin of the secondary relaxations in phenylene polymers, mainly the origin of the so-called γ-relaxation. Covering a broad frequency range (10^{-3}–10^{9} Hz) mechanical (MS) and dielectric (DS) spectroscopy techniques allow a good characterization of the shape and characteristic frequency of secondary relaxations with temperature, but they do not provide microscopic information. To our knowledge the experimental study of molecular motions below the glass transition temperature T_g has been mainly approached by nuclear magnetic resonance (NMR) techniques. Up to date, only very few works[1–3] have exploited neutron scattering (NS) techniques for studying the molecular motions behind the secondary relaxation in polymers. In this direction, we are involved in the study of the problem of sub-T_g molecular motions giving rise to the secondary relaxations in engineering thermoplastics by means of NS techniques.

Numerous MS[4–12] and DS[13–15] experiments in substituted polycarbonates, copolymers, and blends, suggest that the γ-relaxation (located at ~273 K at 1 Hz) is due to the cooperative motion of several units and is closely related to phenylene ring motion. Some p-phenylene polymers present in addition to γ-relaxation, another relaxation—called δ—at even lower temperatures (~100 K and 1 Hz) which is also attributable to motions involving phenylene rings.[10] We note that the rotation of one ring itself would not lead to large dielectric and mechanical losses. Therefore, it seems unlikely to be the origin of the secondary relaxation unless it is cooperatively linked to the motions or is part of the mechanism

[a)]Electronic mail: wapcolej@sq.ehu.es

causing the relaxations and therefore monitoring them, as has been repeatedly suggested in the literature.[13,15–27]

NMR studies of the molecular motions taking place in glassy polycarbonates below T_g show that the main characteristic motions in these systems consist of π-flips of the phenylene rings around the C1C4 axis (see Fig. 1), oscillations of the ring about the same axis, and some small amplitude main-chain reorientation.[16,18,28–32] The activation energy for the flipping process found by NMR correlates well with that obtained from MS and DS for the γ-relaxation. Moreover, polymer structural modifications or the addition of several additives usually have similar effects on the ring motion seen by NMR, and on the secondary γ-relaxation seen by MS or DS.[14,17,22,29,33,34] This correlation has strengthened even more the idea of a close relationship between phenylene ring motion and γ-relaxation. On the other hand, theoretical calculations and molecular dynamics simulations on systems containing phenylene rings qualitatively agree with the type of motions observed experimentally by NMR depending on the time range examined.[25–27,35–40] However, the exact mechanism leading to the occurrence of these flips or the role of the flips on the mechanical properties is not yet clear. There is not a consensus on questions like, up to which extent and in which way do the inter- and intrachain interactions affect the flipping process, or whether the ring flip needs cooperative motion of different units along the chain or not.[7,35,41]

NS is a very suitable technique for the study of dynamic processes from a microscopic point of view, offering both space and time resolution at a molecular level, and allowing a straightforward data interpretation within the framework of the neutron scattering theory.[42,43] In addition, NS together with selective deuteration allows us to highlight the dynamics of a particular atom or molecular group in the system. In contrast to ^{2}H-NMR techniques, the scattering from hydrogen dominates the measured signal in NS. Therefore, using NS we can avoid the possible mass isotope effects of deuterium in ^{2}H-NMR technique, in which deuterium is used to enhance the signal of a particular atom. Moreover, NS allows us to extend the investigation of molecular motions to high frequencies/short time scales, up to 0.1 ps. This can be very useful to study main chain motions and small angle oscillations of phenylene rings, which seem to be very closely related to the mechanism, the flips, and the frictional sliding of chains during deformation.[9,11,18,25,27,36,44–46]

Recently, we have approached the problem of the identification of the molecular motions giving rise to the secondary relaxation below T_g in engineering thermoplastics by means of NS techniques. The final purpose of such a work is to shed new light on the questions discussed above by comparing the sub-T_g dynamics, as observed by NS, in the microscopic (10^{-13}–10^{-11} s) and mesoscopic (10^{-10}–10^{-9} s) time scales for some engineering thermoplastics derived from bisphenol-A (BPA) unit (see Fig. 1). Some preliminary results on the phenylene ring dynamics of BPA polycarbonate (PC) and polysulfone (PSF) in these two windows have recently been published by us.[47,48] In the above-mentioned previous analysis, the existence of differences in the motion of phenylene rings within these two polymers[47,48] became evident. The mentioned preliminary analysis in the mesoscopic[47] and microscopic[48] windows was carried out independently using one model for each time range. Now, in this paper we propose an appropriate model for PSF which describes in a more accurate way the features of the phenylene rings dynamics in both time ranges: microscopic and mesoscopic.

The paper is organized as follows: First, the experimental conditions and a short introduction to NS experiments together with some theoretical aspects of the scattering function for a localized motion are given; thereafter, Sec. III deals with the experimental results obtained for the two time scales and also from diffraction measurements with polarization analysis; in Sec. IV the model is proposed and, finally, the discussion and conclusions are presented in Secs. V and VI.

II. EXPERIMENT

A. Sample

The chemical formula of the studied engineering thermoplastic, PSF of bisphenol-A with deuterated methyl groups ($d6$) is shown in Fig. 1. Molecular weight and polydispersity of the sample supplied by Polymer Source were $M_n = 16\,400$ gr/mol and $M_w/M_n = 1.7$. Differential scanning calorimetry measurements lead to a T_g value of 460 K. Samples were vacuum heated near T_g for 48 h prior to the NS experiments.

B. Neutron scattering experiments

The quantity assessed in a neutron scattering experiment is the double differential cross section: the number of scattered neutrons into a solid angle between Ω and $\Omega + d\Omega$, after having exchanged an energy between E and $E + dE$ with the sample, relative to the number of incident neutrons. The double scattering cross section is expressed in terms of the incoherent $S_\alpha^{\mathrm{inc}}(Q,\omega)$ and coherent $S_\alpha^{\mathrm{coh}}(Q,\omega)$ scattering functions of the different isotopes in the sample as[42,43]

$$\begin{aligned}\frac{\partial^2\sigma}{\partial\Omega\,\partial E} &= \left(\frac{\partial^2\sigma}{\partial\Omega\,\partial E}\right)_{\mathrm{inc}} + \left(\frac{\partial^2\sigma}{\partial\Omega\,\partial E}\right)_{\mathrm{coh}} \\ &= \left(\frac{k}{k_o}\sum_{\alpha}^{\text{species}}\frac{N_\alpha}{4\pi}\sigma_{\mathrm{inc}}^{\alpha}S_\alpha^{\mathrm{inc}}(Q,\omega)\right)_{\mathrm{inc}} \\ &\quad + \left(\frac{k}{k_o}\sum_{\alpha}^{\text{species}}\frac{N_\alpha}{4\pi}\sigma_{\mathrm{coh}}^{\alpha}S_\alpha^{\mathrm{coh}}(Q,\omega)\right)_{\mathrm{coh}} \\ &\quad + \left(\frac{k}{k_o}\sum_{\alpha\neq\beta}^{\text{species}}\sum_{i\alpha\neq j\beta}^{N_\alpha N_\beta} b_{i\alpha}b_{j\beta}\int_{-\infty}^{\infty}\frac{1}{2\pi\hbar}\right. \\ &\quad \left.\times e^{-i\omega t}e^{i\mathbf{Q}[\mathbf{r}_{i\alpha}(t)-\mathbf{r}_{j\beta}(0)]}dt\right)_{\mathrm{coh}}, \end{aligned} \tag{1}$$

where the sums in α and β range over all the different atomic species (O,C,H,D...); the sum in i and j over all the atomic positions; $\mathbf{k}_o$ and $\mathbf{k}$ are the momentum for the incident and scattered neutrons; $\mathbf{Q}$ is the momentum transfer $\mathbf{Q} = \mathbf{k} - \mathbf{k}_o$;

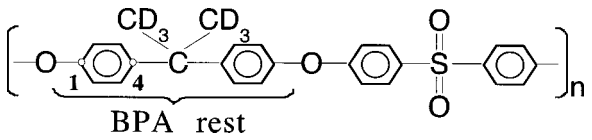

FIG. 1. Molecular formula for polysulfone-*d*6.

$\omega = E/\hbar$; b_i, $\sigma_{\mathrm{coh}}^{\alpha}$, and $\sigma_{\mathrm{inc}}^{\alpha}$ are the so-called scattering length, coherent cross section, and incoherent cross section, respectively, which give the magnitude of the neutron–nucleus interaction; and $\mathbf{r}_i(t)$ is the position of the i nucleus at time t.

The incoherent scattering function $S_{\alpha}^{\mathrm{inc}}(Q,\omega)$ is the Fourier transform of the intermediate scattering function $S_{\alpha}^{\mathrm{inc}}(Q,t)$

$$S_{\alpha}^{\mathrm{inc}}(Q,\omega) = \frac{1}{2\pi\hbar}\int \exp(-i\omega t) S_{\alpha}^{\mathrm{inc}}(Q,t)\,dt. \tag{2}$$

The double Fourier transform of $S_{\alpha}^{\mathrm{inc}}(Q,\omega)$ yields the self part of the Van Hove correlation function, $G_{\mathrm{self}}^{\alpha}(r,t)$, which gives the probability of a given nucleus of kind α to be at a time t at a distance r from its initial position. Thus, incoherent scattering looks at correlations between the positions of the same nucleus at different times. The relation between scattering function and Van Hove function allows a straightforward data interpretation within the framework of the neutron scattering theory. On the other hand, the coherent scattering informs about relative positions of atomic pairs, i.e., collective dynamics. In the static case (diffraction experiment) it reveals the corresponding partial static structure factor. According to Eq. (1), it turns out that the contribution corresponding to the nucleus whose cross section (σ^{α}) is the highest dominates the NS signal. Systems like polymers are usually composed of H, D, C, and O. Hydrogen exhibits a very high value for the incoherent cross section, $\sigma_{\mathrm{inc}}^{H} = 80.27$ barns and, therefore, its scattering dominates the measured intensity. The rest of the coherent and incoherent cross sections—and the mixed products $4\pi b_{i\alpha} b_{j\beta}$—for the nuclei in these systems are much smaller ($\approx$5 barns). Nevertheless, in the most general case the resulting experimental scattering function $I_{\mathrm{exp}}(Q,\omega)$ comprises both coherent and incoherent contributions. As in this work we are interested in the study of the phenylene ring motions, samples with deuterated methyl groups (MG) have been used. In this way, the scattering from MG is strongly suppressed. The total coherent and incoherent scattering cross sections per monomeric unit are 230 and 1297 barns, respectively. On the other hand, the incoherent cross section of the aromatic hydrogen H_{ar} within phenylene rings is 1284 barns/monomer. Thus, the signal is highly dominated by $S_{H_{ar}}^{\mathrm{inc}}(Q,\omega)$. A last general comment on NS spectrometers concerns their limited energy resolution. The measured functions are affected by the instrumental resolution function $R(Q,\omega)$, which is the spectrum that would result after a purely elastic ($\hbar\omega = 0$) scattering event. As a result, the magnitude experimentally determined is

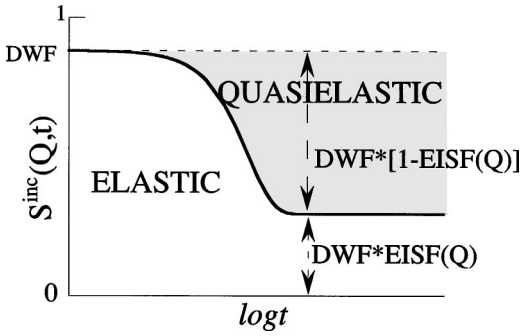

FIG. 2. Schematic representation of an intermediate scattering function for a localized motion. Shadowed area represents the quasiclastic decay due to the motion considered.

$$I_{\mathrm{exp}}(Q,\omega) = \frac{k_o}{k}\left(\frac{\partial^2\sigma}{\partial\Omega\,\partial E}\right) \otimes R(Q,\omega) = I(Q,\omega)\otimes R(Q,\omega). \tag{3}$$

The instrumental resolution function $R(Q,\omega)$ can be determined from the scattering of the sample at very low temperature, where all the dynamic processes are frozen and consequently $I_{\mathrm{exp}}(Q,\omega)$ is proportional to $R(Q,\omega)$

$$R(Q,\omega) = \frac{I_{\mathrm{exp}}(Q,\omega,T\to 0)}{\int_{-\infty}^{\infty} I_{\mathrm{exp}}(Q,\omega,T\to 0)\,d\omega}. \tag{4}$$

The functional form of the incoherent scattering function of Eq. (2) depends on the particular motions we are considering. In a glassy polymer below T_g the atomic motions must be localized in space, since large amplitude correlations do not decay before the setup of the glass transition. The incoherent intermediate scattering function for a localized motion of generic kind "m" has the general expression[42,49]

$$S_m^{\mathrm{inc}}(Q,t) = \mathrm{EISF}_m(Q) + [1-\mathrm{EISF}_m(Q)]\,\phi(t,\Gamma_m), \tag{5}$$

where $\phi(t,\Gamma_m)$ is a normalized relaxation function [$\phi(t=0)=1$ and $\phi(t\to\infty)=0$]; Γ_m is the characteristic frequency of the motion and depends on T; and EISF is the so-called elastic incoherent structure factor. In the most simple case the relaxation function $\phi(t,\Gamma_m)$ is an exponential

$$\phi(t,\Gamma_m) = e^{-t\Gamma_m}, \tag{6}$$

or a Lorentzian function in the frequency domain

$$\phi(\omega,\Gamma_m) = \frac{1}{\pi}\frac{\Gamma_m}{\Gamma_m^2+\omega^2}, \tag{7}$$

if the Fourier transform of Eq. (5) is considered. Figure 2 shows a schematic representation of the generic incoherent intermediate scattering function for a localized motion in the time domain. A Debye–Waller factor (DWF) accounting for the intensity decayed by processes faster than the time scale considered diminishes the measured signal. The EISF(Q) determined by the $t\to\infty$ limit of $S^{\mathrm{inc}}(Q,t)$ (see Fig. 2) gives information about the geometry of the motion.[42,49] For jumps between two equivalent positions at a distance d, the EISF is given by[42]

$$\mathrm{EISF}_{\mathrm{jump}}(Q)=\frac{1}{2}+\frac{1}{2}\left[\frac{\sin(Qd)}{Qd}\right], \tag{8}$$

which is an oscillatory function around 0.5 with the first minimum located at $Q=3\pi/2d$. For instance, in the case of a π-flip of the phenylene ring the aromatic hydrogens (H_{ar}) perform a jump between two equivalent positions separated by a distance $d=4.3$ Å. The EISF corresponding to such a motion displays its first minimum at $Q\sim 1$ Å^{-1}.

1. Diffraction with polarization analysis: D7

Experimentally it is possible to separate the coherent and incoherent contributions to the scattering by using a spin-polarized neutron beam and polarization analysis.[43] The measurements with polarization analysis reported here were carried out by means of the D7 spectrometer at the Institute Laue Langevin (ILL, Grenoble, France). We performed measurements without energy analysis at low (~10 K) and ambient (300 K) temperatures for structural characterization and quantification of the relative contribution of the coherent and incoherent components to the total intensity. This information has been used for the analysis of the measurements with time resolution. The wavelength used at D7 was 4.84 Å, allowing us to cover a Q range $0.16\leqslant Q\leqslant 2.51$ Å^{-1}.

2. Dynamic measurements

Quasielastic NS measurements were carried out in two dynamic windows (microscopic: $\simeq 10^{-13}$–10^{-11} s and mesoscopic: $\simeq 10^{-10}$–10^{-9} s by means of the IN6 time of flight and the IN16 backscattering spectrometers, respectively. Both instruments are also located at the ILL. A flat sample (thickness: 0.26 mm) in an aluminum container was used. The resulting transmission was close to 90%, so that possible multiple scattering contributions could be neglected. Raw data were corrected for the detector efficiency, sample container, and absorption, and also time of flight to energy transfer ($\hbar\omega$) converted, in the case of time-of-flight measurements, by means of the standard programs available at the ILL.

For the time-of-flight (TOF) measurements on IN6 (microscopic time scale) an incident wavelength of 5.12 Å was used; the resulting resolution had a half width at half maximum (HWHM) of about 43 μeV. The scattering angle θ extended from 11.5° to 113.5°. The energy window ranged from ~−2 to some hundreds of meV. The scattering function $I_{\mathrm{exp}}(Q,\omega)$ was obtained from $I_{\mathrm{exp}}(\theta,\omega)$ by means of a standard interpolation program. After this procedure the elastic Q range accessed was $0.32\leqslant Q\leqslant 2$ Å^{-1}. For backscattering measurements (mesoscopic time range) an incident wavelength of 6.27 Å was used, covering a Q range between 0.2 and 1.9 Å^{-1} and an energy window from −15 to 15 μeV with 0.5 μeV (HWHM) resolution.

Energy resolved spectra were recorded at 10 K [for determining $R(Q,\omega)$] and from 50 K up to T_g every 50 K.

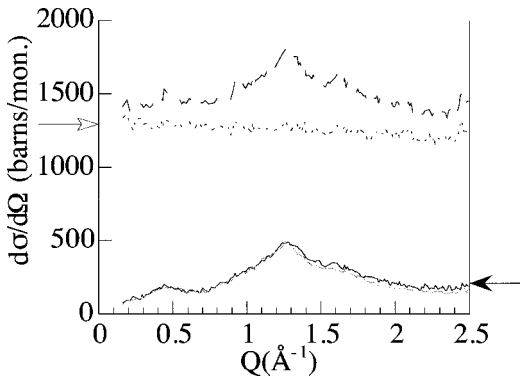

FIG. 3. Total (dashed line, 10 K), incoherent (dotted line, 10 K), and coherent (solid line, 10 K and gray line, 300 K) differential cross sections measured for PSFd6 by D7. The horizontal arrows represent the high-Q limit of the coherent scattering (solid arrow) and the total incoherent cross section (empty arrow).

III. RESULTS

A. D7: Polarization analysis and structural characterization

In an NS experiment without energy analysis, the single differential cross section, $d\sigma/d\Omega$, is measured. It is defined as the integral over the energy of the double differential cross section [Eq. (1)]. D7 measurements resulted in the total (dashed line), incoherent (dotted line), and coherent (solid line) differential cross sections shown in Fig. 3. In the same figure, the arrows indicate the calculated values for the high-Q limit of the coherent scattering, $\Sigma N_\alpha \sigma^\alpha_{\mathrm{coh}}$, and of the incoherent cross section $\Sigma N_\alpha \sigma^\alpha_{\mathrm{inc}}$. The coherent scattering revealing the structural information has a maximum at around $Q_{\mathrm{max}}\sim 1.25$ Å^{-1}. This maximum mainly results from intermolecular correlations at distances $2\pi/Q_{\mathrm{max}}\sim 5$ Å.[50] Another relative maximum at $Q\sim 0.45$ Å^{-1} involving longer correlation distances (on the order of ~14 Å) can also be resolved. The high temperature (300 K) coherent scattering function (gray line in Fig. 3) is very similar to the low temperature one. On the other hand, although hydrogen incoherent scattering dominates the total intensity, this still shows a non-negligible Q-modulation produced by the coherent contribution. As a consequence, to properly reproduce the experimental intensities it will be necessary to introduce coherent contributions when modeling the scattering cross section.

B. IN6: Microscopic timescale

Figure 4 shows the scattering function $I_{\mathrm{exp}}(Q,\omega)$ obtained by means of IN6 for PFSd6 at $Q=1.9$ Å^{-1} and different temperatures. The boson-peak characteristic of glass-forming systems can be identified in the $I_{\mathrm{exp}}(Q,\omega)$ function at energies ~0.9 meV. When moving from lower to higher temperature, a quasielastic contribution appears in $I_{\mathrm{exp}}(Q,\omega)$ filling up the region between the boson peak and the elastic resolution, smearing out the boson peak. On the top of Fig. 4, the mean square displacement (m.s.d. $\langle u^2\rangle$) deduced from the Debye–Waller factor (DWF$=\exp[-\langle u^2\rangle Q^2/3]$) is shown as a function of T. The DWF at each T has been determined from the elastic intensity normalized to the low-T (10 K) elastic intensity. The m.s.d. at low temperatures follows the

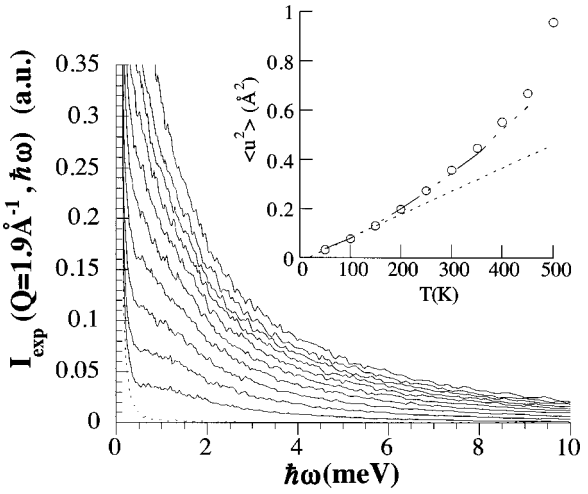

FIG. 4. Scattering function measured on PSFd6 by IN6 at $Q=1.94$ Å^{-1} and at temperatures: 10 K (dashed line) and from 50 to 500 K every 50 K (solid lines from bottom to top). The inset shows the m.s.d. as a function of T. Open circles have been experimentally obtained from the decrease of the elastic intensity (see the text); the dotted and dotted-dashed lines represent the vibrational m.s.d. and the m.s.d. associated with the DWF_{eff}.

linear T dependence characteristic of harmonic vibrations (the extrapolation of the linear fit at $T\leqslant 150$ K is shown in the inset of Fig. 4 by a dotted line). The nonlinear increase of the m.s.d. at $T>200$ K could be attributed to the onset of anharmonic vibrations, to the so-called ''fast dynamics,'' or even to some relaxation process.[51] In order to uncouple phenylene motions from other ''fast dynamic processes'' taking place at times shorter than about 1–2 ps, the $I_{exp}(Q,\omega)$ spectra were Fourier transformed (FT) to the time domain. By this procedure we additionally have the possibility of getting rid of the instrumental resolution effects on the spectra dividing the FT of the scattering function at each temperature, $I_{exp}(Q,t,T)$, by the FT of the scattering function at the lowest temperature measured, $I_{exp}(Q,t,10\,\mathrm{K})$. We thus obtain the intermediate scattering function $S(Q,t)=I_{exp}(Q,t,T)/I_{exp}(Q,t,10\,\mathrm{K})$. Since the temperature dependence of the structure factor is very weak, $S(Q,t)$ is expected to be a normalized function (its value for $t=0$ is 1).

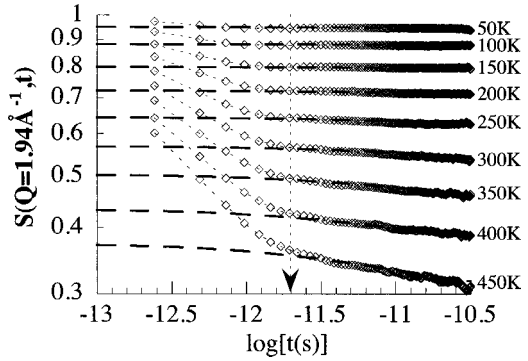

FIG. 5. Intermediate scattering functions obtained from the curves shown in Fig. 4 (same Q and Ts) after being Fourier transformed to the time domain and then divided by the counterpart at 10 K. Dotted lines between experimental points are guides for the eye. Dashed lines are the description obtained with the model proposed for times $t>2$ ps (the limit for applicability of the model is indicated by the vertical arrow).

In Fig. 5 the intermediate scattering functions $S(Q,t)$ corresponding to the curves shown in Fig. 4 are represented as a function of the logarithm of time (logt). All the $S(Q,t)$ exhibit a first steep decay for $t\lesssim 2$ ps due to vibrational and ''fast'' processes. After this first step, for $T<200$ K and times $\gtrsim 2$ ps the $S(Q,t)$ functions stay constant; however, for $T\gtrsim 200$ K a second smooth decay appears for longer times. The motions at $t\gtrsim 2$ ps produce a relatively small decrease of the $S(Q,t)$ function in comparison to that produced by motions faster than 2 ps. Thereby, the increase of the m.s.d. with T, which reflects the decrease of the elastic intensity, is mainly due to motions faster than ~ 2 ps.

The existence of a steep decay in the $S(Q,t)$ at times shorter than ~ 2 ps is not a special characteristic of engineering thermoplastics. Similar results have also been reported for many glassforming systems. This behavior is usually ascribed in the literature to vibrations and fast dynamic processes.[52–63] The origin and characterization of these motions is beyond the scope of the present work. Our goal in this paper is to identify the origin of the second decay of the intermediate scattering function, which may be related to the secondary relaxation processes in PSFd6. Thus, in the following, we will focus on times $t\gtrsim 2$ ps and we will account for vibrations and ''fast processes'' faster than 2 ps with an effective Debye–Waller factor (DWF_{eff}).

The quasielastic decay observed between 2 and 30 ps is very smooth and small in magnitude, less than 0.1 for all T. The relatively high elastic contribution present makes difficult the quantitative analysis of the data through $S(Q,t)$. For this reason, we have characterized the second decay at $t\gtrsim 2$ ps by taking the derivative of the intermediate scattering function. According to Eq. (5) this magnitude reflects the quasielastic features and gives very useful information about the geometry and dynamics of the motion involved. Thus, $S(Q,t)$ has been fitted to a linear function of logt in the time range between 2 and 30 ps, and the slope of the fit has been analyzed as a function of Q and T. Figure 6 displays the absolute value of the slope of the linear fit of $S(Q,t)$ between 2 and 30 ps

$$A(Q,T)=|dS(Q,t)/d\mathrm{logt}|, \tag{9}$$

as a function of temperature for Q values around 0.88 [Fig. 6(a)] and around 1.8 Å^{-1} [Fig. 6(b)]. From this kind of representation, the onset of a process at $T\geqslant 200$ K as well as the setup of the glass transition in the vicinity of 460 K can be easily recognized.

The Q dependence of the quasielastic intensity comprises the spatial information of the motion under consideration. As already mentioned (see the diagram in Fig. 2) this intensity is in addition affected by the decay induced by faster processes. We have taken as a first approach to the DWF_{eff} the $S(Q,t=2\,\mathrm{ps})$ level at different temperatures [intersections between the arrow and the $S(Q,t)$ functions in Fig. 5]. In the following we will call it $DWF_{2\,ps}$. Figure 7 shows the slope of $S(Q,t)$ divided by $DWF_{2\,ps}$ [$B(Q,T)=A(Q,T)/DWF_{2\,ps}$], as a function of Q. The division by $DWF_{2\,ps}$ allows us to remove the Q dependence produced by faster processes from that caused by the motion under investigation [from that of $[1-\mathrm{EISF}(Q)]$ in Eq. (5)]. In the con-

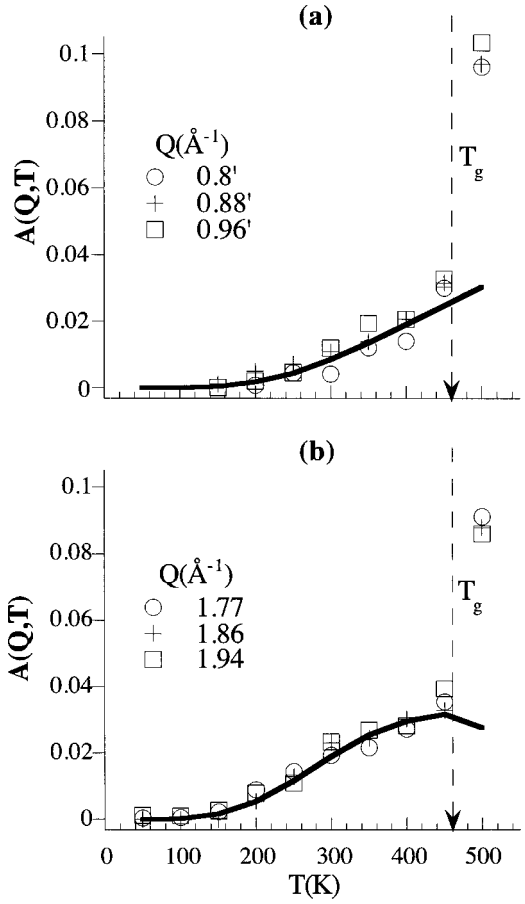

FIG. 6. Calculated (solid lines) and experimental (symbols) $A(Q,T)$ as a function of temperature for $Q\sim0.88\,\text{Å}^{-1}$ (a), and $Q\sim1.8\,\text{Å}^{-1}$ (b). Vertical arrows indicate the glass transition temperature.

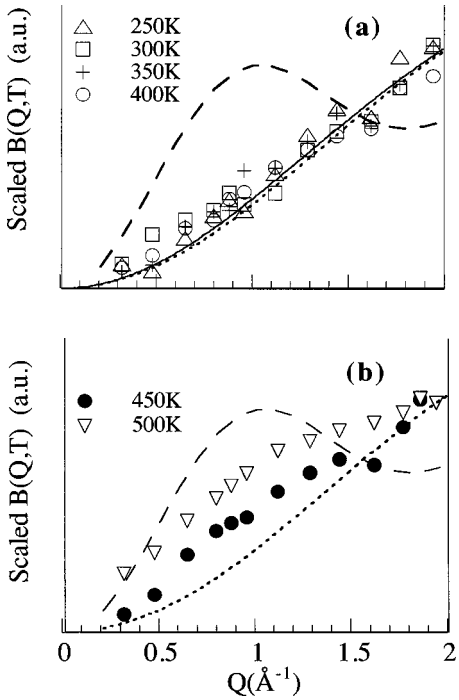

FIG. 7. Scaled $B(Q,T)$ at the various temperatures labeled in the figure. Lines are the [1-EISF(Q)] functions: for jumps between two equivalent positions separated a distance $d\sim4.3\,\text{Å}$ (dashed line) and $d\sim1.5\,\text{Å}$ (dotted line); and for a distribution of jump distances (solid line) resulting from amplitude distributed oscillations of phenylene ring around 0° and width 30°.

struction of Fig. 7, a multiplying factor (consistent with Fig. 6) has been applied to the different temperatures in order to scale all the data to a reference temperature of 300 K. The Q-dependence observed rules out π-flip motion to be the main source of the quasielastic signal in this time/temperature range. As it has been stated above, such a movement would lead to a maximum in the quasielastic intensity via a minimum in EISF(Q) at $Q\sim1\,\text{Å}^{-1}$ (see the dashed line in Fig. 7), which does not agree with the experimental results. On the contrary, the observed Q dependence is compatible with that which would be observed in the case of small distance jumps with $d\sim1.5\,\text{Å}$ (dotted lines in Fig. 7) or small angle oscillations around zero [solid line in Fig. 7(a)]. The extension of this analysis to higher temperatures [Fig. 7(b)] shows a gradual change of the Q shape of $B(Q,T)$. As the temperature increases, a sort of ''hump'' emerges at the position of the maximum of the modulation expected for a π-flip.

C. IN16: Mesoscopic time scale

Figures 8 and 9 show the scattering function $I_{\text{exp}}(Q,\omega)$ of PSFd6 measured in the mesoscopic time scale for several temperatures and Q values. High temperature spectra are clearly broader than the resolution (Fig. 8). Moreover, the extent of the broadening at a given temperature depends on the Q value, the broadening being stronger at $Q\sim1.06\,\text{Å}^{-1}$ than at $Q\sim1.85\,\text{Å}^{-1}$ (Fig. 9). Due to the low values of the quasielastic intensity (Fig. 8 is plotted at a scale ~1% of the maximum value), an analysis involving integrated intensities is more suitable. Thus, we have integrated $S(Q,\omega)$ in different energy ranges: we have defined ''elastic intensity'' as the integral between -2 and 2 μeV; and ''quasielastic intensity'' as the integral between 2 and 5 μeV (shadowed area in Figs. 8 and 9). Figure 10 shows the resulting integrated intensity values as a function of temperature at a constant Q. Several Q values around 0.88 and 1.85 Å^{-1}, respectively, have been depicted to somehow quantify the scattering of the data. The logarithm of the integrated elastic intensity begins to deviate from the linear T dependence corresponding to harmonic vibrations (deduced from TOF elastic data at $T\leqslant150\,\text{K}$ and represented by a dashed line in Fig. 10) at about 200 K (see Fig. 10). Simultaneously, an increase of the integrated quasielastic intensity is observable, indicating the onset of a motion in the dynamic range accessible by IN16. Figure 11 shows, for different temperatures, the ratio between the quasielastic and the total integrated intensities in the IN16 window as a function of Q. In this way, the Q dependence introduced by vibrations and processes faster than the IN16 window is removed. As we have seen before [Eq. (5)], once DWF's Q dependence is eliminated, the quasielastic intensity follows the Q modulation imposed by $[1-\text{EISF}(Q)]$. In contrast to the Q dependence observed in time-of-flight data, here there is a clear maximum at $Q\sim1\,\text{Å}^{-1}$, indicating a larger displacement for the main motion observed in this time scale. In fact, at high temperature the modulation of

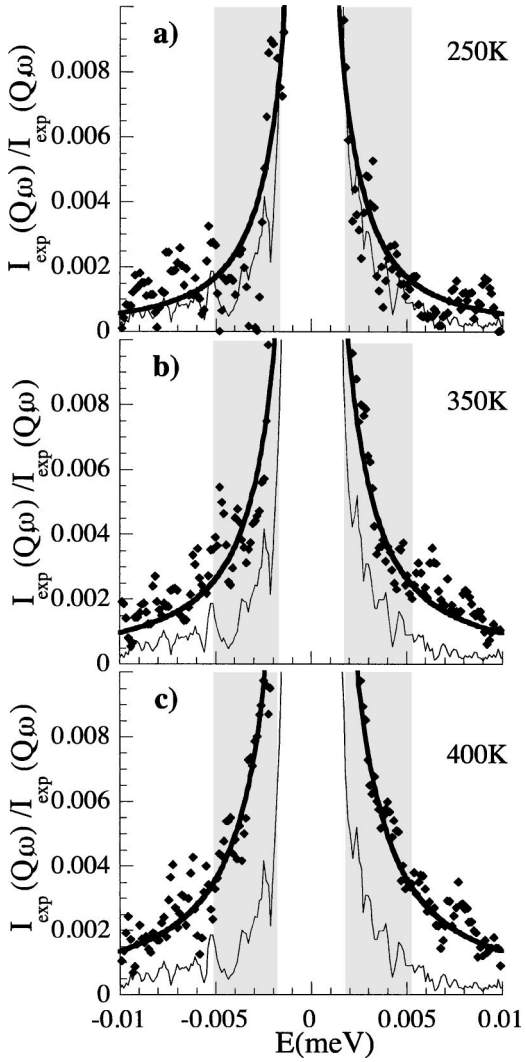

FIG. 8. $I_{exp}(Q,\omega)$ spectra in the mesoscopic time scale measured by IN16 at $Q=0.96$ Å^{-1} for: (a) 250 K; (b) 350 K; and (c) 400 K. The shadowed area encloses the energy range for the quasielastic intensity integration. Thin and thick solid lines represent the experimental resolution and the functions calculated by the model proposed, respectively.

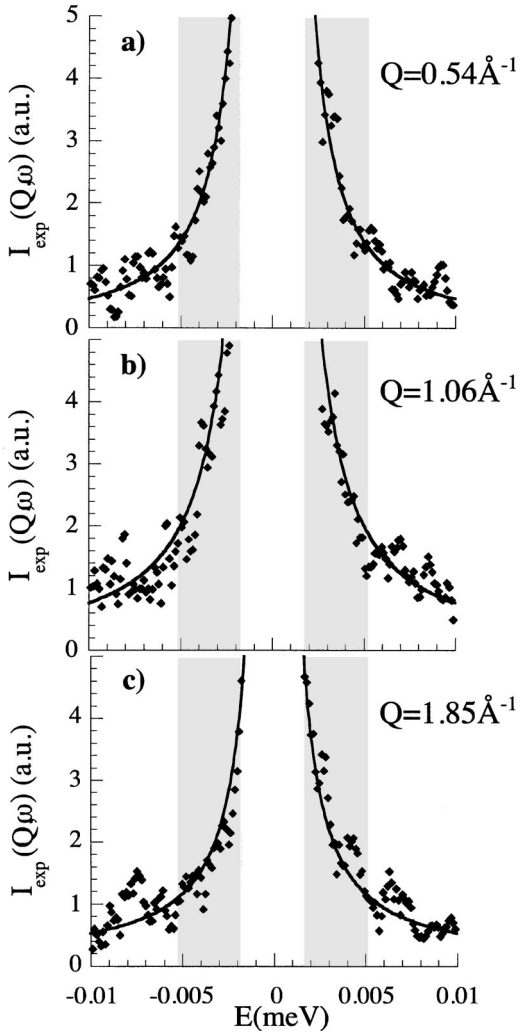

FIG. 9. $I_{exp}(Q,\omega)$ in the mesoscopic time scale measured by IN16 at $T=400$ K for: (a) $Q=0.54$ Å^{-1}; (b) $Q=1.06$ Å^{-1}; and (c) $Q=1.85$ Å^{-1}. Scale: ~2% of the maximum at $Q=1.85$ Å^{-1}. Shadowed area encloses the energy range for the quasielastic intensity integration. Solid lines represent the functions calculated by the model proposed.

these data is compatible with that corresponding to the jump of an H_{ar} participating in a π-flip [that of Eq. (8) with $d=4.3$ Å, dashed line in Fig. 11].

IV. MODEL

A. Proposed scenario

The different geometry (Q modulation) observed for the data in the microscopic and mesoscopic time scales makes clear the existence of at least two different motions. It is known that phenylene rings perform π-flips in several systems with characteristic times that would produce quasielastic broadening in the mesoscopic time scale at $T \gtrsim 300$ K.[16,18,29,32] The obtained Q dependence for the quasielastic intensity in backscattering data (Fig. 11) agrees with that which would be observed in the case of a π-flip motion. Thus, we can identify the main motion observed in the mesoscopic time scale as phenylene π-flips over an energy barrier between two energetically equivalent equilibrium positions. On the other hand, the main motion causing $S(Q,t)$ to decay in the microscopic time scale above 2 ps must involve small displacement of H_{ar}, since the Q modulation in Fig. 7 shows no sign of maximum below $Q \sim 2$ Å^{-1} (at least for $T<450$ K). It is difficult to imagine a relatively fast and low amplitude motion for H_{ar} other than oscillations of the phenylene rings around C1C4 axis or small main chain reorientation. Several NMR investigations by deuteron and C^{13} NMR have already established the need to introduce small angle oscillations in their fast limit in order to better reproduce the measured line shapes.[16,28,30,32] In addition, molecular dynamics simulations and quantum-mechanical calculations show broad distributions of rotational angles around their equilibrium values for phenylene rings,[26,27,36,64–67] indicating that not only one possible equilibrium position exists but a rather broad minimum, and thus, supporting the scenario of fast small amplitude motion within this minimum. The amplitudes proposed in the literature for main chain reorientation[18,37,68] seem to be too small to explain the features observed in our experiments. There-

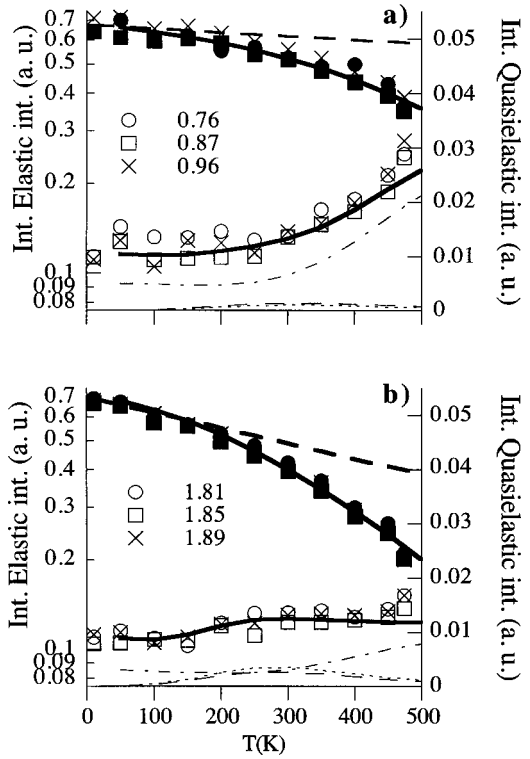

FIG. 10. Temperature dependence of the integrated quasielastic intensity—empty symbols—and integrated elastic intensity—full symbols—for $Q \sim 0.88$ (a) and $Q \sim 1.85$ Å^{-1} (b). The different symbols correspond to the Q values indicated. Thick dashed lines represent the DWF due to harmonic vibrations. Thin solid, dotted-dashed, dotted, and dashed lines are the result of the following calculations, respectively: the integrated elastic and quasielastic intensities (solid lines) and the partial quasielastic contributions of different addenda in Eq. (11) (dotted-dashed line, flip term; dotted line, oscillatory term; dashed line, mixed term).

fore, on the basis of these findings, together with the information available in the literature, we can identify the motion causing the $S(Q,t)$ function to decay at $t \gtrsim 2$ ps as small angle oscillations of variable amplitude around their equilibrium positions. According to what has been observed by NMR measurements, by molecular dynamics simulations,[28,32,66–68] and by our NS experiments, the amplitude of the oscillatory motion would increase with temperature.

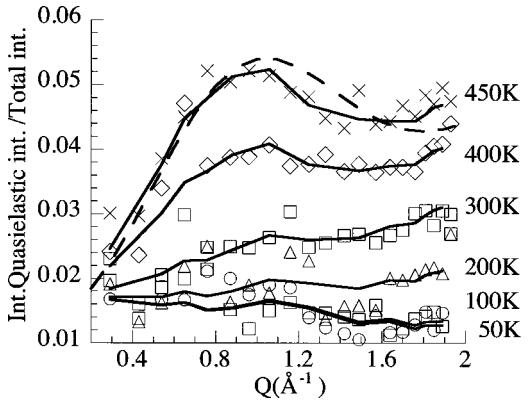

FIG. 11. Q dependence of the integrated quasiclastic intensity normalized to the total intensity in the IN16 window. Different symbols correspond to the different temperatures indicated. The solid lines show the description obtained by the model proposed. The dashed line represents the $[1 - \mathrm{EISF}(Q)]$ for $d = 4.3$ Å scaled arbitrarily to show the Q modulation.

Despite the fact that the main features observed in each time range are different, it is quite common to find in the literature of glassforming systems processes with a broad distribution of characteristic times,[2,3,29,69–72] and as a consequence, we cannot discard the possibility of both motions contributing to both dynamic windows. In fact, if we look for second-order contributions to the main motion in each time scale, they can be perceived indeed. The effect of the main motion detected in the microscopic scale (oscillation) would be most noticeable in the mesoscopic scale at low temperatures (due to the relatively fast characteristic times of the oscillatory motion) and at high Qs (due to the small amplitude of the oscillatory motion). Looking at Fig. 10, we notice that the temperature at which the integrated quasielastic intensity takes off from the resolution level decreases with increasing Q. In Fig. 11 the low temperature data up to ~200 K at low Qs lie in a mess within resolution values, whereas the 200 K curve at high Q clearly stands above the resolution level. On the other hand, the main motion observed in the mesoscopic scale (π-flips) would manifest in the microscopic time scale at high temperatures (when the characteristic times of the flips are shorter) as a stronger decay of the $S(Q,t)$ function and more noticeably at $Q \sim 1$ Å^{-1}, where the maximum modulation for the geometric factor holds. In Fig. 7(b) it is possible to distinguish this still small effect at 450 K and how the modulation clearly changes towards a humped shape at temperatures above T_g.[48] As a consequence, although an independent analysis of the two time scales provides useful information, a proper and more correct description of all the features observed requires a model comprising both motions.

Thus, we present a model scattering function including both π-flips and rapid small angle oscillations of increasing amplitude with T for phenylene ring motion in BPA-PSF. The flip motion would involve the jump of the phenylene ring over an energy barrier between two equivalent positions. On the other hand, oscillations would not encounter any significant barrier but we could think of them just as being caused by rapid fluctuations of the single particle potential seen by the phenylene ring, and produced by the motion of the surrounding atoms.

B. Model function

In the construction of the model we have considered the oscillations and flips of phenylene rings as two statistically independent motions. Under this hypothesis, the total scattering function for an H_{ar} in the time (energy) domain is the product (convolution) of the intermediate scattering functions corresponding to each of the motions [Eq. (5) and its Fourier transform].

$$S^{\mathrm{inc}}_{H_{ar}}(Q,t) = S^{\mathrm{inc}}_{\mathrm{osc}}(Q,t) \cdot S^{\mathrm{inc}}_{\mathrm{flip}}(Q,t). \tag{10}$$

The so-calculated scattering function [Eq. (10)] has several elastic and quasileastic contributions. The quasileastic

intensity, according to the expression of Eq. (5), results in the sum of three relaxation functions weighed by some geometric factors

$$S_{H_{ar,qel}}(Q,t)=\mathrm{EISF}_{\mathrm{flip}}(Q)[1-\mathrm{EISF}_{\mathrm{osc}}(Q)]\phi(t,\Gamma_{\mathrm{osc}})+[1-\mathrm{EISF}_{\mathrm{osc}}(Q)][1-\mathrm{EISF}_{\mathrm{flip}}(Q)]\times\phi(t,\Gamma_{\mathrm{osc}})\cdot\phi(t,\Gamma_{\mathrm{flip}})+\mathrm{EISF}_{\mathrm{osc}}(Q)\times[1-\mathrm{EISF}_{\mathrm{flip}}(Q)]\phi(t,\Gamma_{\mathrm{flip}}). \quad (11)$$

The contribution of each of the terms in Eq. (11) to the total quasielastic signal depends on the characteristic rate Γ_m (m:flip,osc) and Q range chosen. In the previous section, we have based our arguments on the analysis of the experimental data in terms of $I_{\mathrm{exp}}(Q,\omega)$ integrals and $S(Q,t)$ derivatives. The derivative of the intermediate scattering function $dS(Q,t)/d\,\mathrm{log}t$, is a weighed sum of the corresponding derivatives of $\phi(t,\Gamma_m)$ and $\phi(t,\Gamma_{\mathrm{osc}})\cdot\phi(t,\Gamma_{\mathrm{flip}})$, where the weights are the Q-depending geometric factors, $EISF_m\cdot[1-EISF_n(Q)]\ldots$, etc. The temperature dependence of the derivatives of $\phi(t,\Gamma_m)$ and $\phi(t,\Gamma_{\mathrm{osc}})\cdot\phi(t,\Gamma_{\mathrm{flip}})$ functions with respect to logt are smooth curves, each of them showing a broad maximum. When the time scale of the motion is much slower than the times accessible to the spectrometer, i.e., at low Ts, $\phi(t,\Gamma_m)$ stays constant and equal to 1, and therefore its derivative is zero. As the temperature increases and the characteristic time of the motion approaches that of the instrumental resolution, $\phi(t,\Gamma_m)$ starts to decay from 1, leading to a nonzero derivative. As the characteristic time becomes faster, the absolute value of the derivative increases, reaches a maximum, and finally, decreases to zero again when the time scale of the motion is much faster than the times accessible for the spectrometer and $\phi(t,\Gamma_m)$ has completely decayed to zero. Accordingly, when one of the motions is slow enough so that the corresponding function $\phi(t,\Gamma_m)$ function remains constant and equal to 1, we recover for the intermediate scattering function the expression corresponding to one single motion, Eq. (5).

In an equivalent way, the integrals of $\phi(\omega,\Gamma_m)$ and $\phi(\omega,\Gamma_{\mathrm{osc}})\otimes\phi(\omega,\Gamma_{\mathrm{flip}})$ functions in a quasielastic window as a function of temperature will be smooth functions holding a maximum centered at lower or higher temperature depending on the value of the characteristic time $1/\Gamma_m$. When the time scale of the motion is much slower than the times accessible to the spectrometer, $\phi(\omega,\Gamma_m)$ remains narrower than the instrumental resolution and gives no quasielastic integrated intensity. When the characteristic time of the motion approaches that of the instrumental resolution, a nonzero integral appears. With increasing temperature the characteristic time of the motion decreases and $\phi(\omega,\Gamma_m)$ becomes wider and wider. Thus, the quasielastic integral increases more and more, reaches a maximum and finally, decreases when the time scale of the motion becomes much faster than the times accessible for the spectrometer.

According to what it is established for sub-T_g processes we have assumed an Arrhenius-type temperature dependence for both motion rates (Γ_m)

$$\Gamma_m=\Gamma_\infty\exp(-E_a^m/K_BT), \quad (12)$$

with a preexponential factor (Γ_∞) of $10^{13}\,\mathrm{s}^{-1}$ and an activation energy E_a^m.

It is known from several studies in the literature that the dynamics of many sub-T_g processes in glassy systems cannot be described by a single exponential (time domain) or Lorentzian (energy domain) function, but require a certain distribution of characteristic times.[2,3,29,69–72] This distribution of characteristic times would have its origin in the packing heterogeneity at molecular level due to the amorphous character of polymers. The contribution of the intermolecular interactions to the local potential seen by an atom or group of atoms would vary from point to point depending on the local packing. Different local potentials would lead to different characteristic times for a particular motion, but would not change the geometry of the motion itself.[64,73] As a consequence, we have assumed the incoherent scattering of H_{ar} to be the sum of several scattering functions coming from protons in different environments displaying different characteristic times

$$S_{H_{ar}}^{\mathrm{inc}}(Q,t)=\sum_k p_k S_{H_{ar}}^{k,\mathrm{inc}}(Q,t), \quad (13)$$

where $\Sigma_k p_k=1$, and each of the $S_{H_{ar}}^{k,\mathrm{inc}}(Q,t)$ functions is defined as in Eq. (10). The weight p_k would be determined by the distribution of certain undefined structural parameter ξ driving the phenylene dynamics

$$p_k=\int_{\delta\xi}g(\xi)d\xi. \quad (14)$$

The relation between the structural parameter ξ and the local potential defining the characteristic time of the motion would be different for different motions depending on their specific nature, since some motions are more influenced by inter/intramolecular interactions than others. As a consequence, the functional relation between ξ and the local E_a^{osc} and between ξ and the local E_a^{flip} might not be the same. In any case, if the characteristic time of the motion in a certain local environment is parametrized by an activation energy E_a^m, the activation energies will be distributed as well as a result of the intermolecular packing, so that

$$p_k=\int_{\delta E_a^{\mathrm{osc}}}f(E_a^{\mathrm{osc}})dE_a^{\mathrm{osc}}=\int_{\delta E_a^{\mathrm{flip}}}h(E_a^{\mathrm{flip}})dE_a^{\mathrm{flip}}. \quad (15)$$

The interpretation of the distribution in Eq. (13) in terms of packing effects implies that large characteristic times for flips occur in a local environment with large characteristic times for oscillation, and otherwise, low characteristic times for flips occur together with low characteristic times for oscillations. That is, although the two motions have been considered statistically independent, the activation energies for both motions in a certain local environment are assumed to be correlated.

Up to now we have been dealing with the modeling of the incoherent scattering of hydrogen because it dominates the measured scattering cross section [Eq. (1)]. Nevertheless, neutron polarization analysis reveals that it is necessary to introduce coherent contributions as well, to reproduce the experimental intensities. The total coherent signal and the

incoherent signal of atoms other than hydrogen have been considered elastic in a first approximation. In fact, the coherent scattering of motions which do not alter the configuration of the system (such as methyl group threefold rotation or phenyl ring π-flip) are purely elastic. On the other hand, the incoherent scattering cross section of atoms other than hydrogen ($\sigma_{\text{inc}}^{\text{other}}$) is really negligible (13 barns/monomer out of 1297 barns/monomer). Taking into account all these contributions, the scattering function used to describe the data was

$$I^{\text{model}}(Q,t)=\text{DWF}_{\text{eff}}\left[\left(\frac{d\sigma}{d\Omega}\right)_{\text{coh}}+\sigma_{\text{inc}}^{\text{other}}+\sigma_{\text{inc}}^{H}S_{H_{ar}}^{\text{inc}}(Q,t)\right], \tag{16}$$

where $(d\sigma/d\Omega)_{\text{coh}}$ is the coherent differential cross section, and $S_{H_{ar}}^{\text{inc}}(Q,t)$ is that defined in Eq. (13). In order to compare the model and the experimental functions, $I^{\text{model}}(Q,t)$ is normalized to its static (low-T) value, whereas in the energy domain, $I^{\text{model}}(Q,\omega)$ [the energy counterpart of Eq. (16)] is convoluted with $R(Q,\omega)$.

C. Model calculations

The theoretical scattering functions were calculated by means of Eq. (16) together with Eqs. from (5) to (8), (10), (12), and (11). In order to compare the model with the experimental results, the quantities used in Sec. III for data analysis and characterization were obtained. Thus, $A(Q,T)$ and $B(Q,T)$ functions in the microscopic time scale and integrated intensities in the mesoscopic time scale were calculated. As can be appreciated from the inspection of the equations used, there is a relatively large number of parameters involved in the calculation of the model function. However, many of these parameters are fixed within the framework of our model: (i) the scattering cross sections for PSFd6 are those given in section II; (ii) the coherent scattering has been experimentally determined by polarization analysis measurements at D7; and (iii) the EISF(Q) of the slower motion, i.e., $EISF_{\text{flip}}$, is that resulting from a π-flip of a phenylene ring, i.e., that of a jump between two equivalent positions [Eq. (8)] with $d=4.3$ Å. The remaining free parameters are: the DWF_{eff}, the parameters defining the distributions of activation energies for the two motions (which we will call ''dynamic'' parameters), and the EISF(Q) for the small angle oscillations of variable amplitude.

The $\text{EISF}_{\text{osc}}(Q)$ has been parametrized by means of a Gaussian distribution of oscillation amplitudes around 0° of width $\sigma_\theta(T)$. For the dynamic parameters, in a first attempt Gaussian distributions of activation energies for the flip and oscillatory motions were assumed. This leads to a linear relation between E_a^{osc} and E_a^{flip} in each local environment [Eq. (15)] and therefore to the same kind of functional relation with ξ for both activation energies. However, for reproducing experimental data, such a symmetric distribution of E_a^{osc} extended to unphysical negative values of E_a^{osc}. As a consequence, we have used an asymmetric distribution for E_a^{osc} which again has only two parameters

$$f(E_a^{\text{osc}})=\frac{p^p}{\langle E_a^{\text{osc}}\rangle\Gamma(p)}\left(\frac{E_a^{\text{osc}}}{\langle E_a^{\text{osc}}\rangle}\right)^{p-1}e^{pE_a^{\text{osc}}/\langle E_a^{\text{osc}}\rangle}, \tag{17}$$

TABLE I. Dynamic parameters defining the distributions of activation energies for the two motions observed for phenylene rings.

	$\langle E_a\rangle$ (eV)	Variance (eV)
Oscillation	0.22±0.01	0.04
Flips	0.50±0.01	0.11
Oscillation[a]	0.16–0.23	
MG rotation[b]	0.18–0.21	
δ—relaxation[c]	0.19–0.26	

[a]NMR measurements, Ref. 74.
[b]NMR measurements (Refs. 72, 75, 76).
[c]MS measurements, Ref. 10.

where $\Gamma(p)$ is the Gamma function, p determines simultaneously the variance and the asymmetry, and $\langle E_a^{\text{osc}}\rangle$ is the mean value of E_a^{osc}. This kind of distribution is zero for negative values of the E_a^{osc}. For the flips the Gaussian distribution was maintained

$$h(E_a)=\frac{1}{\sqrt{2\pi}\sigma}e^{[-(E_a-\langle E_a\rangle)^2/2\sigma^2]}. \tag{18}$$

The values of the free parameters were determined after an iterative process as follows:

(1) First, from the $Q\sim1.94\,\text{Å}^{-1}$ data in the microscopic time scale, we obtained a first guess for the geometric and dynamic parameters for oscillations $[\langle E_a^{\text{osc}}\rangle,p,\sigma_\theta(T)]$ assuming $\phi_{\text{flip}}(t)$ to be 1. This assumption is quite reasonable because flips are too slow to enter the IN6 window, in view of the Q modulation observed for the microscopic scale data below 450 K (Fig. 7). In addition, at this Q value the coincidence of a minimum for $(1-\text{EISF}_{\text{flip}})$ and the highest $(1-\text{EISF}_{\text{osc}})$ value observable in the Q range accessible, makes the relative weight of ''flip terms'' low. The DWF_{eff} was fixed to $\text{DWF}_{2\text{ ps}}$.
(2) Then, fixing the parametrization of the oscillatory motion as obtained in the previous step, we tested in the mesoscopic time scale at $Q\sim0.88\,\text{Å}^{-1}$ the dynamic parameters for flips $[\langle E_a^{\text{flip}}\rangle,\sigma_{\text{flip}}]$. At that Q value, $(1-\text{EISF}_{\text{flip}})$ is maximum and the relative contribution of oscillations to the quasielastic intensity is minimized due to geometric factors [see Eq. (11)].
(3) The values of the free parameters determined in the previous steps were finally refined by comparison with the experimental data at all Q and temperatures in a sort of iterative process.

This refinement proccess only led to a minor change in the values of the initial parameters. We are aware, of course, that such a procedure implies that there might exist another group of parameters describing the data as well. After this procedure, we estimate a maximum error of 5% for the values obtained. The dynamics parameters found are shown in Table I.

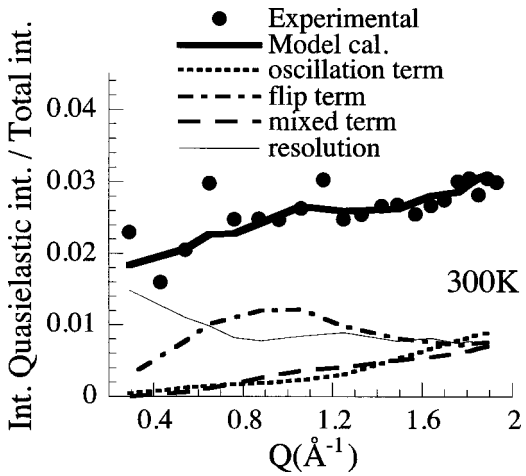

FIG. 12. Experimental (●) and calculated (thick solid line) integrated quasielastic intensities normalized to the total intensity in the IN16 window for $T=300$ K. The dotted-dashed, dotted, and dashed lines represent the partial contributions of the flip, oscillatory, and mixed terms, respectively. The thin solid line represents the resolution.

V. DISCUSSION

All the experimental features are reproduced with high accuracy by the model, as can be seen in Figs. 5 and 6 and 8–11. In Fig. 4 we have depicted the m.s.d. deduced from the $\mathrm{DWF}_{\mathrm{eff}}$. We remind that it gives account for vibrations and other fast processes below ~2 ps. According to the results shown in Fig. 5, the closeness of the total m.s.d. (circles) and the effective m.s.d. (dotted-dashed line) confirms that the motions leading to deviations from the harmonic behavior mainly occur at $t<2$ ps. The difference between the total m.s.d. and the effective m.s.d. reflects the increase of the mobility due to the sub-T_g relaxation processes. It is these processes for which our model is proposed, and therefore the calculated curves in Fig. 5 only aim to describe the experimental results for $t>2$ ps—the faster processes are parametrized by $\mathrm{DWF}_{\mathrm{eff}}$. The calculated intermediate scattering functions describe very nicely the experimental data up to 400 K. We attribute the slight differences at 450 K to the onset of the glass transition. In fact, the values of $A(Q,t)$ at 450 K (Fig. 6) lie off from the general trend for lower temperatures. The trend below T_g is perfectly captured by the model.

Moving to the mesoscopic time scale, Figs. 8 and 9 show the $I^{\mathrm{model}}(Q,\omega)$ functions calculated for several temperatures and Q values. A very good agreement is again found between the theory and the experiment. Not only the Q- but the T dependence of the spectra is described in a very satisfactory way. This is also evidenced when comparing the results in terms of the integrated intensities. The calculated integrated quasielastic and elastic intensities are represented in Fig. 10 with solid lines. Dotted-dashed, dotted, and dashed lines represent the quasielastic contributions from the different terms in Eq. (11): flip, oscillatory, and mixed term, respectively. At intermediate Q values the relatively small geometric factor for $\phi(\omega,\Gamma_{\mathrm{osc}})$ and $\phi(\omega,\Gamma_{\mathrm{osc}})\otimes\phi(\omega,\Gamma_{\mathrm{flip}})$ in Eq. (11) makes the contribution of $\phi(\omega,\Gamma_{\mathrm{flip}})$ dominant. At higher Q values, all the contributions are almost equally important. This can be realized from Figs. 11 and 12 showing the Q dependence of the integrated quasielastic intensity normalized to the total intensity in the IN16 window. In Fig. 12 the partial contributions of the flip, oscillatory, and mixed terms are depicted for $T=300$ K. It is worth mentioning that the consideration of the coherent contributions in the model makes it possible to properly reproduce the observed Q modulation of the normalized quasielastic intensity (see Fig. 11). This is clearly demonstrated for the highest temperature 450 K in Fig. 11. At such a high temperature the modulation of the quasielastic intensity is mainly determined by the π-flip motion (oscillations become too fast to contribute to the IN16 window).

Figures 10, 11, and 12 show that the oscillatory motion really extend to the mesoscopic time scale, and evidence how important is to combine measurements at different time scales to properly interpret and describe the data. If a single motion was producing the quasielastic broadening in the mesoscopic time scale, the T dependence of the integrated quasielastic intensity would be the same for different Q values [factorization in Eq. (5)]. Furthermore, if we considered that the fast motion observed in the microscopic time scale is fast enough to completely decay before entering the IN16 window—i.e., that it produces intensity decay but not quasielastic broadening—we could model it by including the fast motion in an effective DWF for the IN16 spectra: $\mathrm{DWF}_{\mathrm{eff}}^{\mathrm{IN16}}=DWF_{\mathrm{eff}}\cdot\mathrm{EISF}_{\mathrm{osc}}(Q)$ (see Fig. 2). In such a case, the integrated quasielastic intensity normalized to the total integrated intensity in the IN16 window (shown in Fig. 11) would follow just the modulation imposed by the $[1-\mathrm{EISF}(Q)]$ of the slower motion (apart from the slight changes introduced by coherent modulation in the total intensity). However, what we observe is that the modulation imposed by $[1-\mathrm{EISF}_{\mathrm{flip}}(Q)]$ is only followed at high T, where a clear maximum is observed around 1 $\mathrm{Å}^{-1}$, and, in contrast, the low temperature Q dependence is rather different, monotonically increasing with Q rather than showing a maximum (see Fig. 12).

Now, let us discuss the results obtained for the geometric and dynamic parameters of the phenylene ring motions. The Q dependence of the scattering function has allowed us to determine the geometry of the oscillatory motion. The width of the distribution of oscillatory amplitudes around 0° was found to increase with T. This temperature dependence can be described by the power law $\sigma_\theta(T)=0.6T^{0.67}$. For instance, at room temperature we find $\sigma_\theta\sim27°$. On the other hand, the good agreement between theory and experiment concerning the Q dependence of the intensities corroborates the assumption of 180° rotations for the geometry of the slow phenylene ring motion.

Figure 13 shows the distribution of activation energies deduced for oscillations (solid line) and flips (dashed line) and the relationship between E_a^{flip} and E_a^{osc} in the local environments (inset of the figure). Both motions present broad distributions of E_a presumably due to the packing heterogeneity produced by the amorphous character of polymers. The motions, being broadly extended in time through several orders of magnitude, can contribute to the different time windows available in NS instruments. The fact that not only the characteristic time of the flip process is broadly distributed

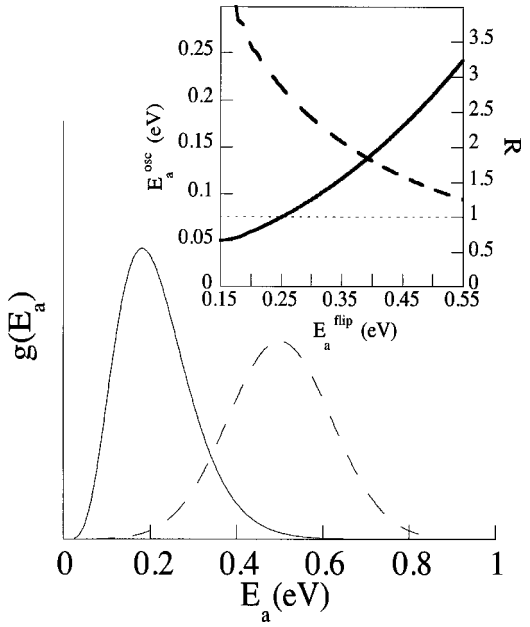

FIG. 13. Activation energy distributions for the flip (dashed line) and oscillatory motion (solid line). Inset: E_α^{osc} (solid line), and R (dashed line) as a function of E_α^{flip}.

but also the characteristic time of the oscillatory motion, is noteworthy. A purely intrachain origin of the small amplitude fast motion should in principle lead to a narrow characteristic time distribution. Equations (14) and (15) show that the ξ derivatives of E_a^m, i.e., the dependence of the activation energy with packing, relate to each other through the relation between E_a^{flip} and E_a^{osc}. This relation is nonlinear (solid line in the inset of Fig. 13), reflecting the fact that the packing affects oscillations and flips in different ways. The dashed line in the inset of Fig. 13 corresponds to the ratio between ξ derivatives of E_a^m, $R=(dE_a^{\mathrm{flip}}/d\xi)/(dE_a^{\mathrm{osc}}/d\xi)=dE_a^{\mathrm{flip}}/dE_a^{\mathrm{osc}}$, experimentally obtained. For small values of the local potential (presumably for low packing) E_a^{flip} depends in a stronger way on the local packing than E_a^{osc} (see the dashed line in the inset of Fig. 13). Nevertheless, for larger potentials (higher packing degree) the oscillatory motion is also affected by packing and R tends to 1. Thus, the broad distribution of characteristic times obtained points to some degree of cooperativity or interchain contribution also for the small amplitude motion. A close relation between the different motions within a polymer, would favor ''lattice'' reorganization, the creation of large motionally activated volume, lower degree of friction during chain sliding,...etc., factors which are believed to benefit mechanical properties.[45,46]

The values found for the dynamic parameters together with other taken from the literature for comparison, are listed in Table I. The mean activation energy $\langle E_a\rangle$ for the flip of the phenylene ring (Fig. 13, Table I) is found to be 0.50 ± 0.01 eV. This value agrees well with those obtained from NMR[30,32,34,71] for the same motion, and also agrees with the apparent $\langle E_a\rangle$ of the γ relaxation observed by MS and DS in similar systems.[6,10,15,77] $\langle E_a\rangle$ for phenylene ring oscillations (Fig. 13, Table I) is noticeably lower than that for the flip. The only experimental reference we found for the E_a of phenylene ring oscillation gave a value between 0.16 and 0.23 eV for PC.[74] On the other hand, Duval *et al.*[53] observed in their TOF-NS data of PC a smooth decay of the intermediate scattering function at times $\gtrsim 2$ ps similar to that observed here. They characterized it in terms of a single characteristic time obtaining, in their own words, a rather imprecise E_a of 0.11 eV, and attributed it to molecular group motions in general.

At this point, we want to note the different physical meaning of the activation energies obtained in the present framework. Whereas the activation energy for flips E_a^{flip} represents a real potential barrier over which phenylene ring jumps, E_a^{osc} does not. In the scenario we propose, oscillations would be caused by rapid fluctuations of the single particle potential. Under this interpretation, E_a^{osc} would measure the barrier of the molecular motions perturbing the single particle potential for phenylene rings. Among all the different molecular motions taking place in PSF, we could consider fast MG rotations and small amplitude main chain motions as a possible origin for such fluctuations. After literature revision, we found interesting the fact that the $\langle E_a\rangle$ for both, MG rotation in PC and PSF (between 0.18 and 0.21 eV)[72,75,76] and the low temperature δ-relaxation in some p-phenylene polymers as seen by MS (between 0.19 and 0.26 eV)[10], are very similar to the $\langle E_a\rangle$ for phenylene ring oscillation. That is, all the different activation energies found in the literature for several fast processes more or less linked to phenylene rings, lie within the distribution of activation energies found here for the oscillatory motion of phenylene rings. Moreover, the characteristic times for MG rotation are also broadly distributed in contrast to what could be expected for a quite local motion.[72,76,78–80] The similarity found for the mean values of the activation energy for ring oscillation and MG rotation, together with the broad distribution of characteristic times observed for both motions, would suggest that both motions are somehow correlated. In agreement with this idea, Bicerano *et al.* found that the energy required for MG rotation in diphenylpropane model compound decreased when little motion of the adjacent phenylene ring was allowed.[36] We interpret that the distribution of E_a^{osc} does not represent a real energy barrier for the phenylene motion, but measures the barriers (or characteristic times) of all the motions causing the local potential to fluctuate. Therefore, the broadening of the distribution would reflect the correlation between ring oscillations and other molecular motions through fast fluctuations of the local potential. The number of works mentioning correlations between different motions in BPA polymers is very high: phenylene ring oscillations and main chain small amplitude motions gating flips, MG rotations in concert with ring oscillations, different phenylene rings separated by the ether or isopropylidene groups flipping simultaneously,...etc. The local motion of a molecular unit, although small in amplitude, would produce via the relations mentioned above far-reaching dynamic fluctuations, the effect of the motion extending to a much larger volume than that covered by the motion itself. This high mobility is probably the key ingredient leading to differences in the mechanical properties between polymers with similar entanglement degree and molecular weight. The activation of differ-

ent conformational motions would reduce steric constraints between chains and therefore reduce the resistance for chains to slide relative to one another when an external stress is applied, and thus, favoring yielding.[45] Moreover, it would prevent nanovoids from stabilization before they could grow in size and form crazes in a kind of competitive kinetic process between nanovoid formation and molecular motion rearrangement.[46]

VI. CONCLUSIONS

The main conclusions of this work can be summarized as follows:

(1) NS is a valuable technique to investigate local molecular motions in polymers deep in the glassy state. The combination of several instruments (time scales) is crucial for a good dynamic characterization of molecular motions.

(2) The fast oscillatory motion seems to emerge from the fluctuation of local phenyl ring environment. Phenylene ring fast oscillations of increased amplitude with T and slower rotations (flips) present broad distribution of characteristic times, extending over several orders of magnitude.

(3) The average time scale of the oscillatory motion for phenylene rings is very close to those found for MG rotation and δ relaxation in similar polymers. This facts suggest: on the one hand, some kind of cooperativity between MG rotation and phenyl ring motion, which would favor mechanical properties, and on the other hand, that those oscillations, and/or the motions intimately linked to them, may be the molecular origin of the mechanic low-T δ-relaxation.

(4) The activation energies found for phenylene ring π-flips agree well with that found for MS γ relaxation in symilar systems, confirming one more time their close relation and suporting a role for phenylene ring motion in mechanical properties. Nevertheless, when comparing the average time scale for the phenylene π-flips with the literature results on the time scale of the γ relaxation, it is found that, despite the rather different values reported, the phenylene ring motions are systematically slower. This would evidence that other faster molecular motions are also relevant for determining the good mechanical properties of this type of engineering thermoplastics γ relaxation.

ACKNOWLEDGMENTS

We acknowledge The Basque Government, ''Donostia International Physics Center,'' Iberdrola S.A., and the support of the following research projects: DGICYT, PB97-0638; GV, EX 1999-11; UPV/EHU, 206.215-G20/98. S. Arrese-Igor also acknowledges the grant of the Basque Government.

[1] G. Meier, F. Fujara, and W. Petry, Macromolecules **22**, 4421 (1989).
[2] A. Arbe, D. Richter, J. Colmenero, and B. Farago, Phys. Rev. E **54**, 3853 (1996).
[3] A. Arbe, J. Colmenero, B. Frick, M. Mokenbusch, and D. Richter, Macromolecules **31**, 4926 (1998).
[4] A. F. Yee and S. A. Smith, Macromolecules **14**, 54 (1981).
[5] J. R. Fried, A. Letton, and W. J. Welsh, *Order in the Amorphous State of Polymers*, edited by S. E. Keinath, R. L. Miller, and J. K. Rieke (Plenum, New York and London, 1987).
[6] J. R. Fried, A. Letton, and W. J. Welsh, Polymer **31**, 1032 (1990).
[7] C. L. Aitken, J. S. McHattie, and D. R. Paul, Macromolecules **25**, 2910 (1992).
[8] P. L. Lee, T. Kowalewski, M. D. Poliks, and J. Shaefer, Macromolecules **28**, 2476 (1995).
[9] C. J. G. Plummer, C. L. Soles, C. Xiao, J. Wu, H. H. Kausch, and A. F. Yee, Macromolecules **28**, 7157 (1995).
[10] L. David, C. Girard, R. Dolmzon, M. Albrand, and S. Etienne, Macromolecules **29**, 8343 (1996).
[11] C. Xiao, J. Wu, L. Yang, F. Yee, L. Xie, D. Gidley, K. L. Ngai, and A. K. Rizos, Macromolecules **32**, 7913 (1999).
[12] J. Liu, J. M. Goetz, J. Schaefer, A. F. Yee, and L. Li, Macromolecules **34**, 2559 (2001).
[13] G. Katana, F. Kramer, E. W. Fischer, and R. Plaetschke, Macromolecules **26**, 3075 (1993).
[14] A. K. Rizos, L. Petihakis, K. L. Ngai, J. Wu, and A. F. Yee, Macromolecules **32**, 7921 (1999).
[15] A. S. Merenga, C. M. Papadakis, F. Kremer, J. Liu, and A. F. Yee, Macromolecules **34**, 76 (2001).
[16] J. Shaefer, E. O. Stejskal, R. A. McKay, and W. T. Dixon, Macromolecules **14**, 1479 (1984).
[17] C. J. T. Landry and P. M. Henrichs, Macromolecules **22**, 2157 (1989).
[18] M. D. Poliks, T. Gullion, and J. Schaefer, Macromolecules **23**, 2678 (1990).
[19] J. H. Walton, M. J. Lizak, M. S. Conradi, T. Gullion, and J. Schaefer, Macromolecules **23**, 416 (1990).
[20] D. Schaefer, M. Hansen, B. Blmich, and H. W. Spiess, J. Non-Cryst. Solids **131**, 777 (1991).
[21] M. T. Hansen, A. S. Kulik, K. O. Prins, and H. W. Spiess, Polymer **33**, 2231 (1992).
[22] C. A. Klung, J. Wu, C. Xiao, A. F. Yee, and J. Schaefer, Macromolecules **30**, 6302 (1997).
[23] J. M. Goetz, J. Wu, A. F. Yee, and J. Schaefer, Macromolecules **31**, 3016 (1998).
[24] J. Shaefer, E. O. Stejskal, D. Perchak, J. Skolnick, and R. Yaris, Macromolecules **18**, 368 (1985).
[25] D. Perchak, J. Skolnick, and R. Yaris, Macromolecules **20**, 121 (1987).
[26] J. H. Dhih and C. L. Chen, Macromolecules **28**, 4509 (1995).
[27] D. R. Whitney and R. Yaris, Macromolecules **30**, 1741 (1997).
[28] H. W. Spiess, Colloid Polym. Sci. **261**, 193 (1983).
[29] J. J. Dumais, A. L. Cholli, L. W. Jelinski, J. L. Hedrick, and J. E. McGrath, Macromolecules **19**, 1884 (1986).
[30] A. K. Roy, A. A. Jones, and P. T. Inglefield, Macromolecules **19**, 1356 (1986).
[31] P. B. Smith, R. A. Bubeck, and S. E. Bales, Macromolecules **21**, 2058 (1988).
[32] J. F. Shi, P. T. Inglefield, A. A. Jones, and M. D. Meadows, Macromolecules **29**, 605 (1996).
[33] F. J. Hörth, K. J. Kuhn, and J. Mertes, Polymer **33**, 1223 (1992).
[34] M. Wehrle, G. P. Hellmann, and H. W. Spiess, Colloid Polym. Sci. **265**, 265 (1987).
[35] J. Liu, A. F. Yee, J. M. Goetz, and J. Schaefer, Macromolecules **33**, 6849 (2000).
[36] J. Bizerano and H. A. Clark, Macromolecules **21**, 585 (1988).
[37] M. Hutnik, A. S. Argon, and A. W. Suter, Macromolecules **24**, 5970 (1991).
[38] C. F. Fan, T. Çagin, W. Shi, and K. A. Smith, Macromol. Theory Simul. **6**, 83 (1997).
[39] Y. J. Sung, C. L. Chen, and A. C. Su, Macromolecules **24**, 6123 (1991).
[40] S. F. Tsai, I. K. Lan, and C. L. Chen, Comput. Theor. Polym. Sci. **8**, 283 (1998).
[41] C. Xiao and A. F. Yee, Macromolecules **25**, 6800 (1992).
[42] M. Bée, *Quasielastic Neutron Scattering* (Hilger, Bristol).
[43] S. W. Lovesey, *Theory of Neutron Scattering from Condensed Matter* (Clarendon, Oxford, 1984).
[44] P. M. Henrichs, H. R. Luss, and R. P. Scaringe, Macromolecules **22**, 2731 (1989).
[45] L. P. Chen, A. F. Yee, and E. J. Moskala, Macromolecules **32**, 5944 (1999).
[46] J. Liu and A. F. Yee, Macromolecules **33**, 1338 (2000).
[47] S. Arrese-Igor, A. Arbe, A. Alegría, B. Frick, and J. Colmencro, Appl. Phys. A: Mater. Sci. Process. **7**, 454 (2002).

[48] S. Arrese-Igor, A. Arbe, A. Alegría, B. Frick, and J. Colmenero, Chem. Phys. **292**, 363 (2003).
[49] M. Béc, Physica B **182**, 323 (1992).
[50] B. Frick, D. Richter, and Cl. Ritter, Europhys. Lett. **9**, 557 (1989).
[51] R. Zorn, A. Arbe, J. Colmenero, B. Frick, D. Richter, and U. Buchenau, Phys. Rev. E **52**, 781 (1995).
[52] U. Buchenau, C. Schönfeld, D. Richter, T. Kanaya, K. Kaji, and R. Wchrmann, Phys. Rev. Lett. **73**, 2344 (1994).
[53] L. Saviot, E. Duval, J. F. Jal, and A. J. Dianoux, Eur. Phys. J. B **17**, 661 (2000).
[54] F. Fujara and W. Petry, Europhys. Lett. **4**, 921 (1987).
[55] W. Knaak, F. Mezei, and B. Farago, Europhys. Lett. **7**, 529 (1988).
[56] W. Doster, S. Cusack, and W. Petry, Phys. Rev. Lett. **65**, 1080 (1990).
[57] J. Wuttke, M. Kiebel, E. Bartsch, F. Fujara, W. Petry, and H. Sillescu, Z. Phys. B: Condens. Matter **91**, 357 (1993).
[58] J. Colmenero, A. Arbe, and A. Alegría, Phys. Rev. Lett. **71**, 2603 (1993).
[59] R. Zorn, A. Arbe, J. Colmenero, B. Frick, D. Richter, and U. Buchenau, Phys. Rev. E **52**, 781 (1995).
[60] T. Kanaya, T. Kawaguchi, and K. Kaji, J. Chem. Phys. **104**, 3841 (1996).
[61] E. Kartini, M. F. Collins, B. Collier, F. Mezei, and E. C. Svensson, Phys. Rev. B **54**, 6292 (1996).
[62] U. Buchenau, A. Wischnewski, D. Richter, and B. Frick, Phys. Rev. Lett. **77**, 4035 (1997).
[63] J. Colmenero and A. Arbe, Phys. Rev. B **57**, 13508 (1998).
[64] M. Hutnik, F. T. Gentile, P. J. Ludovice, A. S. Argon, and A. W. Suter, Macromolecules **24**, 5962 (1991).
[65] C. L. Chen, H. L. Chen, and J. H. Shih, Macromolecules **27**, 2087 (1994).
[66] C. L. Chen, C. L. Lee, H. L. Chen, and J. H. Shih, Macromolecules **27**, 7872 (1994).
[67] T. Shi, W. Jiang, L. An, and B. Li, Macromol. Theory Simul. **10**, 232 (2001).
[68] A. D. English, Macromolecules **17**, 2182 (1984).
[69] A. J. Moreno, A. Alegría, J. Colmenero, M. Prager, H. Grimm, and B. Frick, J. Chem. Phys. **115**, 8958 (2001).
[70] A. J. Moreno, A. Alegría, J. Colmenero, R. Mukhopadyay, and B. Frick, J. Non-Cryst. Solids **287**, 242 (2001).
[71] H. Kaji, T. Tai, and F. Horii, Macromolecules **34**, 6318 (2001).
[72] P. M. Henrich and V. A. Nicely, Macromolecules **24**, 2506 (1991).
[73] C. F. Fan and S. L. Hsu, Macromolecules **24**, 6244 (1991).
[74] M. Wehrle, Dissertation, University of Mainz (1986).
[75] C. Schmidt, K. J. Kuhn, and H. W. Spiess, Colloid Polym. Sci. **71**, 71 (1985).
[76] D. Fernandez, J. M. Alberdi, and J. Colmenero (personal communication) (2003).
[77] L. P. Chen, A. F. Yee, J. M. Goetz, and J. Schaefer, Macromolecules **31**, 5371 (1998).
[78] A. Chahid, A. Alegría, and J. Colmenero, Macromolecules **27**, 3282 (1994).
[79] J. Colmenero, R. Mukhopadhyay, A. Alegría, and B. Frick, Phys. Rev. Lett. **80**, 2350 (1998).
[80] A. J. Moreno, A. Alegría, J. Colmenero, and B. Frick, Macromolecules **34**, 4886 (2001).